

Effect of operation regime on bubble size and void fraction in a bubble column with porous sparger

Shahrouz Mohagheghian¹, Afshin J. Ghajar¹, and Brian Elbing¹

¹Oklahoma State University System

May 5, 2020

Abstract

Performance of bubble columns under transport processes is dependent on bubble size distribution and void fraction. These multiphase parameters are sensitive to the operation regime of a bubble column. The current work presents a systematic study of bubble size and void fraction in a batch bubble column within the homogeneous and heterogeneous regimes. Effect of liquid viscosity and gas superficial velocity on bubble size distribution, void fraction, and operation regime was investigated. Results showed that increasing the viscosity accelerates the regime transition. Bubble size distributions were statistically characterized using probability density function and probability plots. It was shown that bubble size distribution shifts from near-Gaussian in the homogenous regime to lognormal (in parts) in the heterogeneous regime. Dimensional reasoning was used to scale the bubble size and void fraction with respect to the operation regime.

Transport Phenomena and Fluid Mechanics

Effect of operation regime on bubble size and void fraction in a bubble column with porous sparger

Shahrouz Mohagheghian^a, **Afshin J. Ghajar**^b, & **Brian R. Elbing**^c

School of Mechanical and Aerospace Engineering, Oklahoma State University

201 General Academic Building, Oklahoma State University, Stillwater, OK 74078

^amohaghe@okstate.edu, ^bafshin.ghajar@okstate.edu, & ^celbing@okstate.edu

Submitted to the AIChE Journal

Abstract

Performance of bubble columns under transport processes is dependent on bubble size distribution and void fraction. These multiphase parameters are sensitive to the operation regime of a bubble column. The current work presents a systematic study of bubble size and void fraction in a batch bubble column within the homogeneous and heterogeneous regimes. Effect of liquid viscosity and gas superficial velocity on bubble size distribution, void fraction, and operation regime was investigated. Results showed that increasing the viscosity accelerates the regime transition. Bubble size distributions were statistically characterized using probability density function and probability plots. It was shown that bubble size distribution shifts from near-Gaussian in the homogenous regime to lognormal (in parts) in the heterogeneous regime. Dimensional reasoning was used to scale the bubble size and void fraction with respect to the operation regime.

Keywords : Operation Regime, Bubble Size Distribution, Bubble Size Scaling, Void Fraction Scaling, Liquid Viscosity.

Introduction

Bubble columns are commonly used as contact reactors in chemical processing, bio-chemical, and metallurgical applications due to their simplicity (e.g., no moving parts), low operation cost, and high efficiency at heat and mass transfer. Understanding and modeling the transport phenomena as well as hydrodynamics of bubble columns requires a fundamental understanding of characteristics of the dispersed (gas) phase (i.e. bubbles). Bubble size (d_b), population, and rise velocity (U_b) significantly influence the physical behavior of the bubbly flow.¹ Bubble size distribution (BSD) is a primary aspect in the understanding of the physical behavior of the multiphase flow and was studied in this work. Note that the bubble rise velocity is a function of bubble size; therefore, any factor that effects the bubble size effects the rise velocity, which in turn effects the void fraction (ϵ). Both bubble size and void fraction are impacted by gas superficial velocity, liquid properties, bubble column operation condition, column geometry, and gas injection method. Current work studies the effect of gas superficial velocity and liquid viscosity on bubble size and void fraction.

Shah et al.² showed that the void fraction is predominately a function of the gas superficial velocity. The study of bubble columns with different system characteristics showed that there is a direct correlation between gas superficial velocity and void fraction.³⁻¹¹ Lockett and Kirkpatrick¹² and Kara et al.¹³ showed that in the homogenous regime, void fraction exhibits a linear increase with increasing gas superficial velocity. However, in the heterogeneous regime the functional form between gas superficial velocity and void fraction is less apparent.^{13,14} Liquid properties effect the void fraction by influencing the bubble formation as well as coalescence and breakup processes.¹ The bubble column literature reports both increasing and decreasing void fraction with increasing liquid viscosity.¹⁵⁻²¹ Besagni et al.²² argues that viscosity has a dual effect on void fraction. At low liquid viscosity, the coalescence is limited and increasing the viscosity increases the drag force acting on bubbles and, in turn, increases the bubble residence time and void fraction. However, in more viscous liquids, viscosity increases the coalescence rate and, consequently, produces larger bubbles with higher terminal velocity that decrease the void fraction. Bubble column literature provides numerous correlations for the prediction of the void fraction. Interested readers are referred to Besagni et al.²³ for a summary of available correlations. Akita and Yoshida²⁴ proposed a well-known correlation for void fraction scaling based on dimensional analysis. Their work suggests that the Froude number (Fr), Archimedes number (Ar), and Eötvös number (Eu) scale the void fraction with a power law functional form, $\epsilon/(1-\epsilon)^4 = C \rho^X \mu^Y \sigma^Z$. Here C is a proportionality constant and X, Y, Z are the powers of each non-dimensional term. Similar functional forms are reported in the bubble column literature.^{16,25-28} Akita and Yoshida²⁴ used the column diameter as a characteristic length scale to calculate the aforementioned dimensionless terms; however, in the present study using the bubble size as the characteristic length scale seems more appropriate since the bubble size is much smaller than the column diameter.

There is a general scarcity in bubble size data reported in the bubble column literature, partly because of the difficulties associated with bubble size measurements. While Leonard et al.²⁹ outline the inconsistencies in the bubble size distribution literature, there is a general consensus that in the homogenous regime the bubble sizes increase with increasing the gas superficial velocity while in the heterogeneous regime bubble size decreases with increasing the gas superficial velocity. Li and Prakash³⁰ studied the spatial distribution of bubbles and found that smaller bubbles dominate the near wall region, and larger bubbles are more common in the central region of the column. In a highly viscous liquid, the bubble surface is more stable, larger bubbles form at the injector,^{31,32} and the coalescence rate is larger than the breakage rate.^{2,33-35} The study of bubble size distribution shows that in viscous liquids the probability density function (PDF) of the BSD exhibits a bimodal shape.^{15,21,36,37} In the bubble column literature, scaling of the characteristic bubble length has been broadly approached assuming the sizing is dominated by either a breakage mechanism³⁸ or bubble formation.^{39,40} The former attempts to find a stable bubble size under a given external (breakage)

force in the heterogeneous regime, and the latter aims to find a characteristic bubble length scale in the homogenous regime using gravity, surface tension, and shear forces acting on a bubble.

The goal of the current work is to study the bubble size and void fraction in a batch bubble column with respect to operation regime and contribute to the current understanding of these multiphase parameters. This paper is organized as follows. Section 2 describes the experimental setup including instrumentation used. In Section 3, the results are presented for characterization and scaling of the bubble size and void fraction. Finally, conclusions and remarks on the current work are given in Section 4.

Experimental Methods

2.1 Bubble column

The bubble column was made from cast acrylic to achieve strength and optical clarity; it was 1.2m in length with a 102mm internal diameter (D). Figure 1 provides a schematic of the bubble column test facility. Tap water was passed through a cartridge filter (W10-BC, American Plumber, Pentair Residential Filtration, LCC) with $5\mu\text{m}$ nominal filtration. Surface tension of the filtered water and other tested liquids were measured with a force tesiometer (K6, Krüss GmbH) and platinum ring (RI0111-282438, Krüss GmbH). Over several days the surface tension of the filtered water was measured to be $72.6 \pm 0.4 \text{ mN/m}$, which is comparable to the nominal surface tension of the pure water ($\sim 72.8 \text{ mN/m}$). Liquid phase temperature was measured using a thermocouple (HSTC-TT-K-20S-120-SMPW-CC, Omega Engineering). Figure 1 also depicts the compressed airflow control panel. Airflow passes through a cartridge filter (SGY-AIR9JH, Kobalt, Lowe's Companies, Inc.) with $5\mu\text{m}$ nominal filtration. The mass flow of air was controlled and monitored with a combination of a pressure regulator, rotameter (EW-32461-50, Cole-Palmer), and a thermocouple (5SC-TT-K-40-39, Omega Engineering). The rotameter measured the volumetric flow of air with an accuracy of 2% of the full scale (FS). The thermocouple measured the air temperature immediately upstream of the rotameter with accuracy of $\pm 0.1^\circ\text{C}$. All tests were conducted with the air temperature between 20°C and 22°C , and temperature difference between the air and liquid phase was within $\pm 2^\circ\text{C}$. It is also worth mentioning that the height of liquid in the bubble column was kept constant at $9D$ following recommendations from Besagni et al.⁴¹ for studying the void fraction and bubble size independent of column aspect ratio.

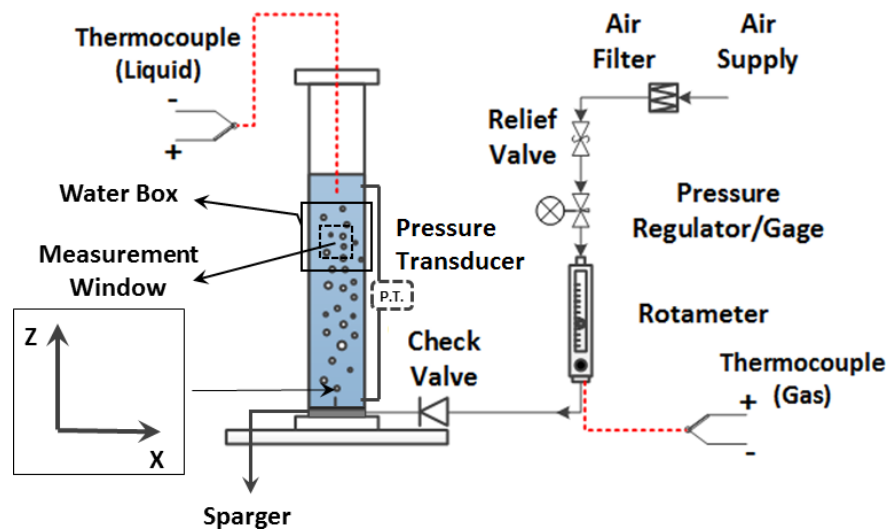


Figure 1 . Schematic of the experimental setup including the bubble column and airflow control and monitoring system.

The air sparger was comprised of a porous air stone covering $\sim 90\%$ of the cross-section of the column that was mounted on a cylindrical plenum. The porous air stone was fed from a 350 ml plenum, which used porous material identical to the air stone to supply pressure drop for cross-sectional uniformity of air injection. The sparger was designed to be pressurized up to 7 bar. A differential pressure transducer (PX2300-DI, OMEGA) measured the pressure drop within the line supplying the plenum. BSD depends heavily on the average pore size in a homogenous bubbly flow. The average pore size (r_p) was calculated from

$$\overline{r_p} = \frac{2\sigma}{p_{cap}}, \quad (1)$$

where σ is the surface tension and $[?]/p_{cap}$ is the differential pressure measured across the sparger at the onset of bubbling. Equation (1) was adopted from Houghton et al.,⁴² which explains that the $[?]/p_{cap}$ measured in the aforementioned fashion represents the average capillary pressure at the onset of bubbly. In the current work the average pore size was $85\mu\text{m} \pm 10\mu\text{m}$.

The refraction index mismatch as well as the round geometry of the acrylic column introduced a significant optical distortion. Thus a refractive index matching box (water-box) was used to mitigate this problem. The water-box was $0.2\text{m} \times 0.15\text{m} \times 0.15\text{m}$, made from casted acrylic, and filled with water. Spatial calibration was performed with a custom calibration plate, and the residual image distortion after mounting the water-box was negligible relative to the bubble sizes measured.

2.2 Bubble size measurement

A camera (EOS 70D DSLR, Canon) was used to capture monochrome still images of the bubbles. This camera had an APS-C CMOS image sensor ($22.5\text{mm} \times 15\text{mm}$) with a maximum resolution of 5472×3648 pixels. The camera pixel size was $4.1\mu\text{m} \times 4.1\mu\text{m}$ with a 14-bit depth. The camera was fitted with a 60 mm 1:2.8 lens (Canon) to produce a nominal field-of-view of 120 mm by 80 mm. The column was backlit with an LED panel (Daylight 1200, Fovigtec StudioPRO) that delivered up to 13,900-illumination flux (5600 K color temperature) at one meter. Backlighting was uniformly diffused using a 3 mm thick white acrylic sheet. Homogenous backlighting simplifies image-processing as well as improves the measurement accuracy. Bubble images were processed for bubble size measurements using ImageJ (1.49v, National Institutes of Health (NIH), Bethesda, MD, USA),⁴³⁻⁴⁶ a common open access image-processing program. Within ImageJ, an edge detection algorithm was used to sharpen the bubble edges, subtract the background, and apply a grayscale threshold to convert the 14-bit images to binary images. A subset of images from each condition were manually processed and then used to determine the appropriate grayscale threshold. It is worth mentioning that the bubble images become darker in background as the number of bubbles per image increases. Therefore, a range of acceptable threshold values were explored for each condition and produced a 2% variation in measured bubble size. Interested readers are referred to the previous studies from the current research group⁴⁷⁻⁴⁹ for more details on the image processing scheme. Including uncertainty from the spatial calibration and image processing procedures, the measurement uncertainty was less than 8%. In the current work, the imaging system and processing scheme could resolve bubbles as small as 0.2 mm in diameter. Figure 2 provides an example of a bubble image with the identified bubbles using the appropriate threshold outlined. Figure 2 also depicts that the processing algorithm can identify in-focus bubbles and exclude out-of-focus bubbles, which minimizes the impact of out-of-plane bubble locations on the spatial calibration. In addition, Figure 2 shows that, even with a proper threshold, overlapping and defective bubbles can contaminate the size distributions. Consequently, each image was manually inspected for the aforementioned problems and impacted bubbles were removed from the population sample.

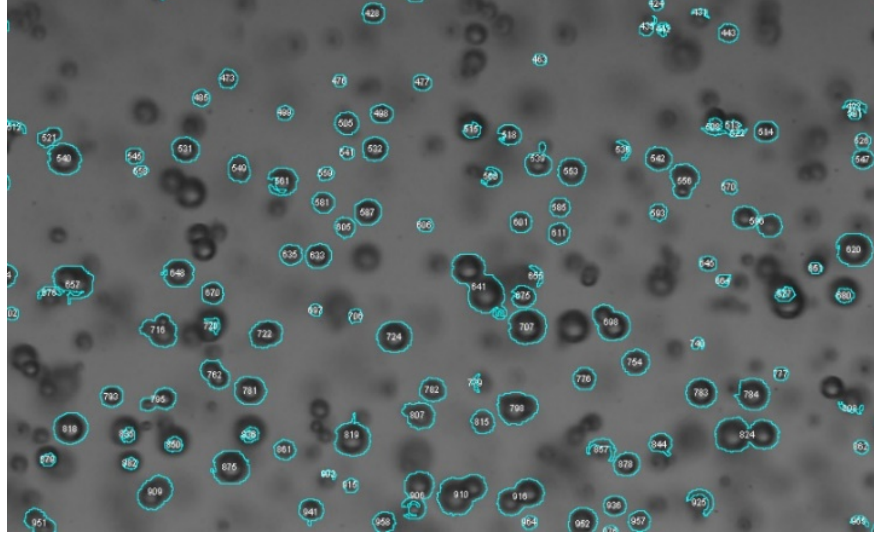


Figure 2 . Sample of processed bubble-image using ImageJ for bubble size measurements. Identified bubbles have contour lines around them.

Bubbles were approximated by ellipsoids in shape, and Equation (2) was used to determine the equivalent diameter (d_{eq}) of a sphere with the same cross-sectional area (A_b), which was used as the bubble size representative length. Here a is the major bubble axis and AR is the aspect ratio of the bubble. The cross-sectional area, bubble centroid location, and the aspect ratio were calculated for each identified bubble in ImageJ. This equivalent bubble diameter was used in Equation (3) to compute the Sauter mean diameter (d_{32}), which is the ratio of the representative bubble volume to the bubble surface area and is a common measure of the average bubble size.

$$d_{eq} = \sqrt{\frac{a^2}{AR}} \quad (2)$$

$$d_{32} = \frac{\sum_{i=1}^n d_i^3}{\sum_{i=1}^n d_i^2} \quad (3)$$

2.3 Void fraction measurement

Void fraction is defined as the ratio of gas volume to the total volume of the system. In the current work, void fraction was calculated from the differential pressure ($[?]p$) along the column height during operation. A differential pressure transducer (PX2300-DI, OMEGA) was employed to obtain the hydrostatic pressure between two pressure taps with a separation of $8D$ along the column height (see Figure 1). A data acquisition card (National Instruments, USB-6218 BNC) was used to acquire the output signal from the pressure transducer and the signal was recorded on a desktop computer (via LabVIEW 15.0.1). Here the uncertainty associated with the pressure measurement was calculated to be under 2% of the measured value for all cases tested. Void fraction was calculated using Equation (4), where $[?]H$ is the vertical distance between the pressure taps, ρ_L and ρ_G are the density of liquid and gas, respectively, and g is gravitational acceleration.

$$\varepsilon = \frac{p}{(\rho_L - \rho_G)gH} \quad (4)$$

2.4 Test matrix

Table 1 provides the test matrix for examining the effect of liquid properties as well as gas superficial velocity ($\Upsilon_{\Sigma\Gamma}=4X_{\Gamma}/\pi\Delta^2$) on multiphase parameters (e.g. bubble size and void fraction). To explore the effect of liquid properties on bubble size and void fraction, aqueous solutions of glycerin with different concentrations were tested. In the current work, the range of the liquid viscosity tested was in excess of two orders of magnitude, while the surface tension and density were changed by only about 10% and 20%, respectively, relative to that of water.

Table 1 . Test matrix for liquid phase properties (at 20 °C) and gas superficial velocities.

Index	Liquid phase	μ_A (Pa.s)	ρ_A (kg/m ³)	σ (mN/m)	U_{SG} (mm/s)
<i>G1</i>	Glycerin 85%	0.161	1224	0.065	6.9, 13.8, 20.7, 27.6, 34.4, 41.4, 48.3, 55.2, 62, 69
<i>G2</i>	Glycerin 79%	0.083	1208	0.065	
<i>G3</i>	Glycerin 60%	0.016	1157	0.067	
<i>W</i>	Water	0.001	998	0.072	

Results and Discussion

3.1 Regime identification

The objective was to find a threshold for the transient gas superficial velocity and study the effect of viscosity on this threshold. BSD characteristics and higher order statistics (skewness and kurtosis) were used to identify the operation regimes. Figure 3 shows the probability density function (PDF) of bubble size in aqueous solutions of glycerin (*G1* and *G3*, see Table 1) at various superficial gas velocities. Figure 3 shows that as the gas superficial velocity exceeds 27.6 mm/s in both cases the PDF shape changes from a bell shape into a spike shape; bubble column literature^{24,40} attributed the aforementioned shift in PDF shape to regime alternation from homogenous to heterogeneous regime. In addition, Figure 3a shows that the lower gas superficial velocities ($U_{SG} [?] 27.6$ mm/s) exhibit a bimodal shape in the PDF, this feature has been reported in studies of the homogenous operation regime in the bubble column literature.^{15,21,36,37} In homogenous bubbly flow with no bubble breakage and coalescence events, the injection condition (i.e. pore size and gas superficial velocity) determines the bubble size. The pore size distribution on the sparger is discrete and non-monodisperse, which explains the deviation of bubble size distribution from a truly Gaussian distribution. Higher order statistics (skewness and kurtosis) of the BSD were obtained for further inspection of the operation regime shift. Table 2 presents the Sauter mean diameter (d_{32}), (arithmetic) mean diameter (d_{10}), standard deviation (RMS), as well as higher order statistics of BSD in *G1* at the gas superficial velocities tested. Skewness (S) and kurtosis (κ) of the bubble size distribution in Table 2 show a significant deviation from a Gaussian-distribution ($S \sim 0, \kappa \sim 3$) when the gas superficial velocity exceeds $U_{SG} = 27.6$ mm/s.

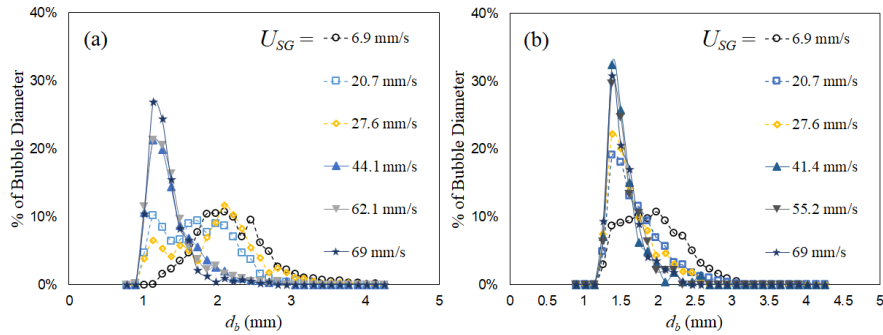


Figure 3 . Probability density function (PDF) of bubble size in (a) G1 and (b) G3.

Table 2 . Bubble size and statistics at various gas superficial velocities tested in G1.

U_{SG} (mm/s)	d_{32} (mm)	d_{10} (mm)	$RMS(d_b)$ (mm)	$S(d_b)$	$\kappa(d_b)$
6.9	2.4	2.2	0.5	0.8	4.3
20.7	2.3	2.1	0.5	0.5	3.4
27.6	2.3	2.0	0.6	0.5	4.0
41.4	2.2	1.8	0.6	1.4	6.4
55.2	1.7	1.4	0.4	2.3	12.2
62.1	1.8	1.4	0.4	3.3	20.0
69.0	1.5	1.4	0.4	4.2	28.4

So far it was discussed that the homogenous operation regime exhibits Gaussian-like characteristics and heterogeneous regime features a spike shape distribution; this was inspected using PDF plots of BSD from the range tested (see Table 1). Figure 4 shows the bubble size distribution from G1 plotted on probability coordinates. Figure 4a shows that in homogenous range (based on gas superficial velocity) the BSD exhibits linearity on a normal distribution probability plot. The near-Gaussian behavior in the homogenous regime was also discussed above by means of the PDF shape and higher order statistics. BSD from heterogeneous operation cases (41.4 mm/s U_{SG} 69 mm/s) in G1 was plotted on a lognormal probability plot (see Figure 4b). It is interesting to see the strong linear behavior of BSD on a lognormal probability plot. Figure 4b also shows that the range at which the BSD exhibit linear trend on a lognormal probability plot starts at the mode of the PDF (thick solid vertical line) and ends at the Sauter mean diameter (d_{32} , vertical lines). The mode of the PDF corresponds to the most frequent bubble size, d_{mf} , interested reader can refer to Mohagheghian and Elbing⁴⁷ for analysis of d_{mf} . The present study shows that only a portion of the right leg of the BSD PDF within heterogeneous regime is lognormal. The PDF exhibits a linear trend between d_{min} and d_{mf} ; furthermore, the PDF can be modeled with a second order polynomial curve between d_{32} and d_{max} .

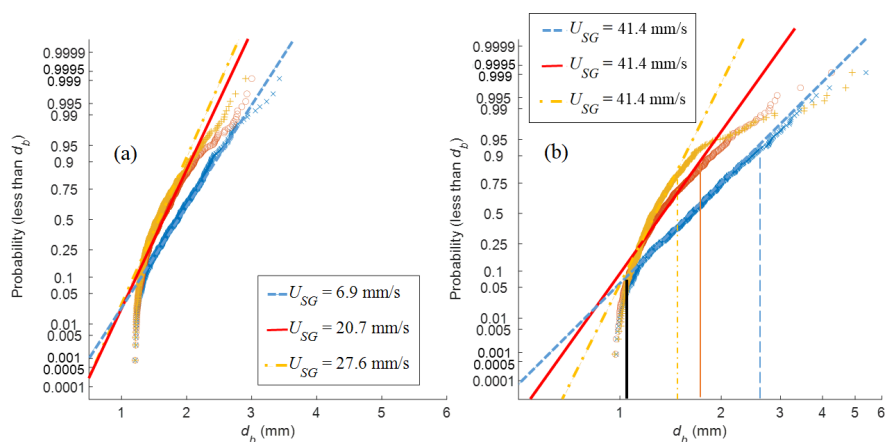


Figure 4 . Probability plots of BSD with G1 in the (a) homogenous regime; 6.9 mm/s U_{SG} 27.6 mm/s on a normal probability plot and (b) heterogeneous regime; 41.4 mm/s U_{SG} 69 mm/s on a lognormal probability plot.

Figure 5 presents the PDF of the bubble size at different viscosities (see Table 1) illustrating the sensitivity of BSD to the viscosity of the liquid phase. Once the gas superficial velocity is sufficiently high (in this case $U_{SG} = 27.6$ mm/s), the viscosity modifies the near-Gaussian distribution (in water) to a spike shape distribution.

It was discussed that the shift in the distribution shape is an indication of operation regime change from homogenous to heterogeneous. Manual inspections showed that, increasing the viscosity reduces the bubble terminal velocity due to friction drag; moreover, increasing the viscosity effects the bubble motion by creating planar oscillations in the bubbles trajectory, these two effects in turn enhance the bubble coalescence, this results in the formation of larger bubbles that are more susceptible to shear breakage. At higher gas superficial velocities, the number of coalescence and breakage events increases; therefore, the BSD shape shifts towards a spike (lognormal distribution) and the standard deviation decreases (i.e. distribution narrows). In summary, increasing the viscosity modifies the BSD, and increases bubble-wake interactions; these effects, alter the physical structure of the bubbly flow from homogenous to heterogeneous.

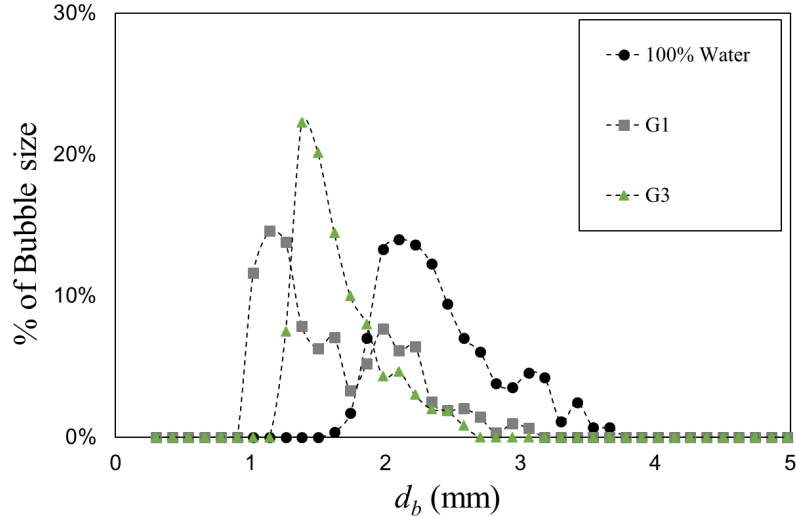


Figure 5 . Probability density function of bubble size at different liquid viscosities and $U_{SG} = 27.6$ mm/s.

Transport coefficients determine the performance and efficiency of a bubble column and are sensitive to the bubble size and void fraction. Bubble size and void fraction are heavily depended on the operation regime, which sets the dominant fluidic mechanisms within a gas-liquid system. The rest of this paper is structured as such to study the bubble size and void fraction with respect to the operation regimes i.e., homogenous and heterogeneous.

3.2 Homogeneous regime

In this section bubble size and void fraction were studied in the homogenous operation regime, which features a linear trend between the void fraction and the gas superficial velocity as well as a direct correlation between bubble size and gas superficial velocity. Homogeneous bubbly flow is characterized by the absence of breakage and coalescence and a Gaussian BSD; therefore, any attempt to scale the bubble size should include the pore size (r_p) and the gas superficial velocity (U_{SG}) in the parameter space. The present work also includes the liquid properties (i.e. surface tension σ , liquid viscosity μ_A , and liquid density ρ_A), and gravity (g) to scale the bubble size in the homogenous regime. Using dimensional analysis, the scaled bubble size was expected to be dependent on the Froude number (Fr), Weber number (We), and Reynolds number (Re); see Equations (5)-(7).

Figure 6 validates the correlation for predicting bubble size (d_{32}) in homogeneous regime (see Equation 8) against experimental bubble size data. Results show that in the homogenous regime the proposed correlation predicts the bubble size. In Equation (8) the power exponents were found following the recommendation

from Kazakis et al.,⁴⁰ which argues that the sparger material effects correlations of this type due to the sensitivity of bubble size to pore dimensions in homogeneous bubbly flow. The power law functional form between the aforementioned non-dimensional terms (see Equations 5-7) was first suggested by Akita and Yoshida;²⁴ in addition, in Equations (5)-(7) the exponents were obtained empirically.⁴⁰

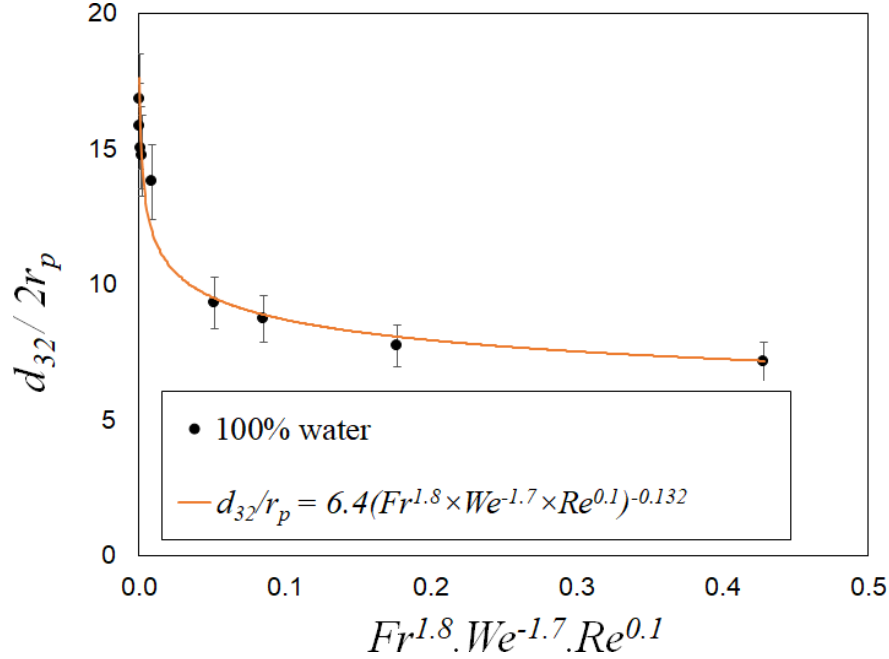


Figure 6 . Scaled bubble size in homogenous regime (water).

$Fr = \frac{U_{SG}}{\sqrt{gd_{32}}}$	(FroudeNumber)	(5)
$We = \frac{U_{SG}^2 \rho d_{32}}{\sigma}$	(Weber Number)	(6)
$Re = \frac{\rho_L d_{32} U_{SG}}{\mu_L}$	(ReynoldsNumber)	(7)
$\frac{d_{32}}{2r_p} = 6.4 (Fr^{1.8} We^{-1.7} Re^{0.7})^{-0.132}$	$\frac{d_{32}}{2r_p} = 6.4 (Fr^{1.8} We^{-1.7} Re^{0.7})^{-0.132}$	(8)

Figure 7 shows the void fraction from the tested conditions in the present work, there is a direct correlation between void fraction and gas superficial velocity. It was argued in the previous section that regime shift from homogeneous to heterogeneous operation regime can be identified from higher order statistics and probability density plots. Here, it was attempted to investigate the regime change at similar gas superficial velocity ($USG = 27.6$ mm/s) using void fraction data. Figure 7 shows that above $USG = 27.6$ mm/s, void fraction (ϵ) deviates from the linear trend with gas superficial velocity, which indicates that the homogeneous regime was no longer present. Figure 7 also shows that for the highest viscosity tested (G1) the void fraction levels off after $USG = 27.6$ mm/s. Detailed observations of the bubble column showed that the void fraction in G1 tests levels off due to a significant drop in gas residence time (data not shown). In these cases, the relatively high gas superficial velocity results in formation of slugs from bubble coalescence near the sparger; these slugs are unstable and travel significantly faster than bubbles and, consequently, the gas residence time decreases.²² However, in the rest of the cases tested in Figure 7 (i.e. G3 and water) the void fraction increases with gas superficial velocity.

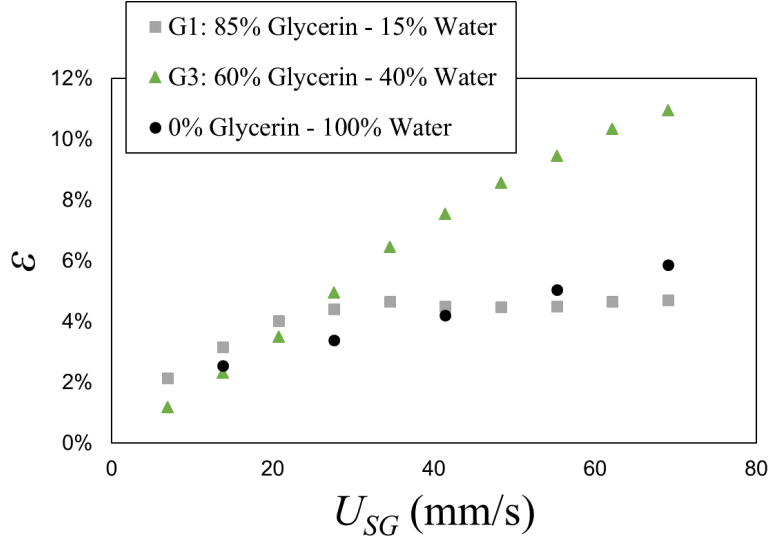


Figure 7 . Void fraction measurement in water and different aqueous solutions of glycerin (G1 and G3).

A parameter space was identified via careful inspection of the experimental setup to formulate a correlation to predict the void fraction using dimensional analysis. It was concluded that the parameter space should be comprised of liquid properties (i.e. surface tension, viscosity, and density), external body force (i.e. gravity), bubble size (d_{32}), and the gas flow rate (i.e. gas superficial velocity). The effect of gas superficial velocity, gravity, and liquid properties were accounted for using Froude number (Equation 5), Archimedes number (Equation 9), and Eötvös number (Equation 10) for scaling the void fraction. Equation (11) shows the resulting correlation for scaling the void fraction, where $G(\cdot)$ is an unknown function. Following Akita and Yoshida,²⁴ Mouza et al.,³⁹ Kazakis et al.,⁴⁰ and Anastasiou et al.,⁵⁰ a power law functional form was considered for the unknown function G . Figure 8 validates the correlation for predicting the void fraction (ϵ) in homogeneous regime against experimental data showing that Equation (12) successfully predicts the void fraction within $\pm 5\%$ accuracy of the current measurements.

$\text{Ar} = \frac{d_{32}^3 \rho_L g}{\mu_L^2}$	(Archimedes Number)	(9)
$\text{Eo} = \frac{d_{32}^2 \rho_L g}{\sigma}$	(Eötvös Number)	(10)
$\epsilon = G(\text{Fr}, \text{Ar}, \text{Eo})$	$\epsilon = G(\text{Fr}, \text{Ar}, \text{Eo})$	(11)
$\epsilon = 0.0278 (\text{Fr}^{1.117} \text{Ar}^{0.1} \text{Eo}^{-0.032})^{0.4959}$	$\epsilon = 0.0278 (\text{Fr}^{1.117} \text{Ar}^{0.1} \text{Eo}^{-0.032})^{0.4959}$	(12)

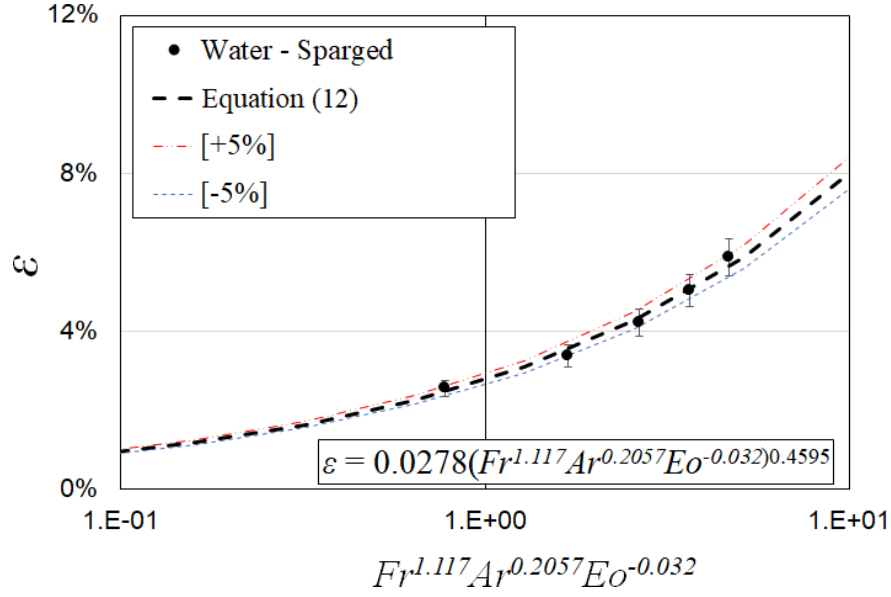


Figure 8 . A correlation for scaling the void fraction in the homogenous regime (water).

3.3 Heterogeneous regime

The heterogeneous operation regime features frequent breakup and coalescence events. Coalescence produces larger bubbles, which are more susceptible to deformation and breakage. Generally, coalescence increases the number of large bubbles and breakage increases the number of small bubbles; therefore, in a statistically stationary bubble size population the coalescence skews the PDF negatively (towards the right tail) and breakage skews the PDF positively (towards the left tail). This explains the shift in PDF shape from a bell (hump) shape to a positively skewed spike shape when the operation regime changes from homogenous to heterogeneous regime. To approach the physical scaling of the bubble size characteristic length scale, it was hypothesized that in heterogeneous regime the interfacial momentum transfer sets the stable bubble size. Therefore, the energy supplied to the liquid phase from the injection of the gas phase is expected to power the interfacial momentum transfer. In the current work, statistically stationary samples of bubble size were used to test this hypothesis. Sauter mean diameter was measured according to the test matrix in Table 1 to test the relationship between bubble size and specific input power per unit mass ($P_m = gU_{SG}$). Hinze³⁸ studied the breakage of drops and recommended using the maximum stable drop size (d_{95}) under shear breakage for scaling and argues that d_{95} is the characteristic length that constrains 95% of the dispersed phase volume. Alves et al.⁵¹ argue that the Sauter mean diameter is proportional to the maximum stable bubble size; therefore, in the present work d_{32} was used as the bubble size characteristic length scale for bubble size scaling. Figure 9 shows the measured d_{32} at various P_m levels, which shows that for the glycerin conditions (G1-G3) the Sauter mean diameter decreases with increasing specific input power. Hinze³⁸ proposed a correlation (Equation 13) to predict the maximum stable bubble size as a function of specific power input, surface tension, and density of the continuous phase. In Equation (13), the proportionality coefficient (k) is a function of the critical Weber number (We_{cr}). It has been demonstrated that the proportionality constant corresponds to different mechanisms, including $k = 0.725$ for isotropic turbulent³⁸ and $k \sim 1.7$ for shear bubble breakup.^{52,53} Figure 9 compares the predicted bubble size from Equation (13) ($k = 0.45$) with the measured bubble size (Sauter mean diameter) from all cases tested in the present study.

$$d_{32} = k \frac{\left(\frac{\sigma}{\rho_L}\right)^{3/5}}{P_m^{2/5}} \quad (13)$$

The non-dimensional form of Equation (13) was produced using dimensional analysis on the given parameter space, which results in a single non-dimensional term equal to proportionality constant (k). If this is repeated with the addition of viscosity (μ_L) into the parameter space, then Equation (14) relates the bubble size (d_{32}) with the input power ($P_m = gU_{SG}$) and liquid properties (surface tension, liquid viscosity, and liquid density). Equation (14) suggests that the unknown functional form $f()$ needs to be found experimentally from bubble size (d_{32}) data. Detailed inspections show that at lower specific input powers the bubble column is still operating in the homogenous regime; consequently, in the absence of shear breakage bubble size cannot be predicted from Equation (13). Figure 9 also shows that the d_{32} from conditions tested in water increase with increasing gas superficial velocity (specific input power), this is due to homogenous operation regime. The non-dimensional terms in Equation (14) are well established dimensionless terms; the scaled bubble size (left hand side) is the Ohnesorge number (Oh), which is the ratio of the product of the inertia and surface tension forces to viscous forces. The scaled specific input power, which is related to the shear breakage, is the product of the Morton number ($Mo = \frac{g\mu_L^4}{\rho_L\sigma^3}$) and the Capillary number ($Ca = \frac{\mu_L U_{SG}}{\sigma}$); here the scaled P_m term is a combination of viscous, inertia, surface tension, and gravitational forces.

$$\frac{\rho_L d_{32} \sigma}{\mu_L^2} = f\left(\frac{P_m \mu_L^5}{\rho_L \sigma^4}\right) \quad (14)$$

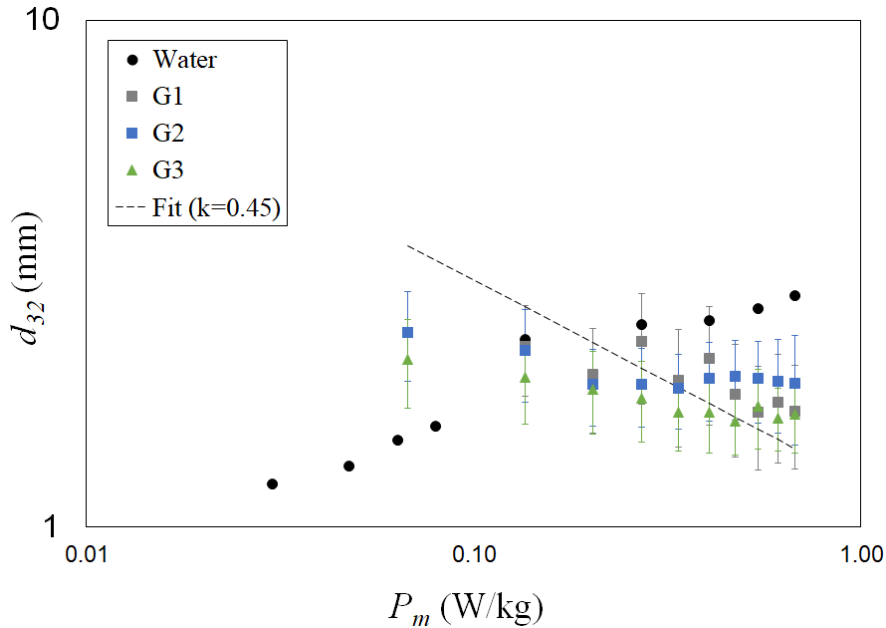


Figure 9 . Bubble size (Sauter mean diameter) measurement in water and different aqueous solutions of glycerin.

It was attempted to find the functional form $f()$ between the scaled bubble size and scaled specific input power in Equation (14). Hinze³⁸ suggested a power law correlation (Equation 15) between the scaled bubble size and scaled specific input power. The current study found a power law correlation with similar power (slopes) to that of Hinze³⁸ (see Equation 16). Bubble size measurements from Mohagheghian and Elbing⁴⁷ were used for further validation of Equation (16). Note that Mohagheghian and Elbing⁴⁷ measurements were carried out in the same test facility; however, a single point air injection method was used for bubbling the column. Figure 10 shows that data from the present study, Hinze,³⁸ and Mohagheghian and Elbing⁴⁷ collapse on Equation (16) (dashed black line). To further examine the present correlation for scaling the bubble size, similar studies^{39,40} were used to check validity of the present correlation.

$$\frac{\rho_L d_{32} \sigma}{\mu_L^2} = 0.725 \left(\frac{P_m \mu_L^5}{\rho_L \sigma^4} \right)^{-0.4} \quad (15)$$

$$\frac{\rho_L d_{32} \sigma}{\mu_L^2} = 0.2477 \left(\frac{P_m \mu_L^5}{\rho_L \sigma^4} \right)^{-0.4} \quad (16)$$

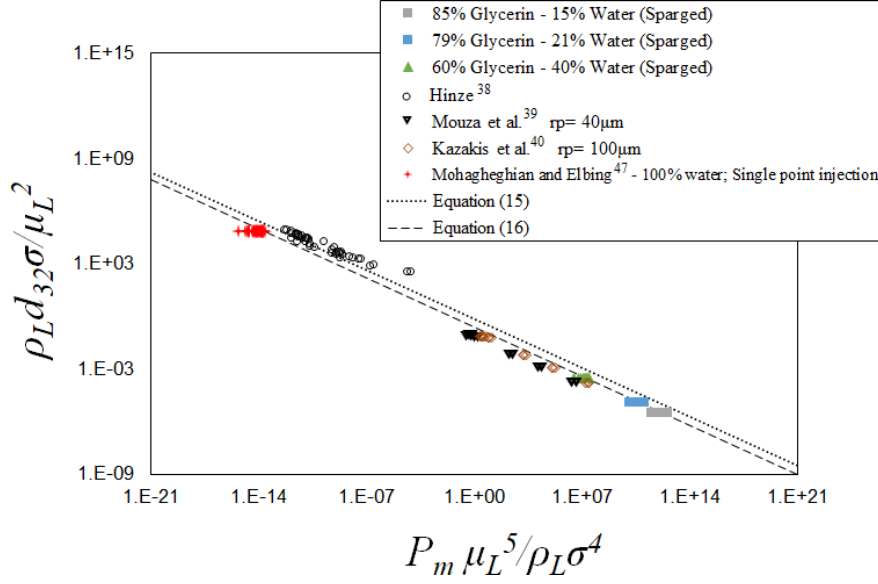


Figure 10 . Scaled bubble size versus scaled specific input power using results from the literature in addition to the current study.

In the rest of this section void fraction measurements and scaling in heterogeneous regime are discussed. The same parameter space for producing Equation (11) was employed for scaling the void fraction and finding the function form of $G()$. Here, it was assumed that the bubbles are traveling at terminal velocity (see Figure 11); therefore, the drag force ($F_D \propto \rho_A \delta_{32}^2 \Upsilon_\beta^2$) was balanced with buoyancy force ($\Phi_B = \rho_A \gamma \delta_{32}^3$). This assumption establishes a relationship between bubble size and bubble velocity ($U_b^2 \sim g d_{32}^3$). It is known that the void fraction is the ratio of gas superficial velocity to the bubble velocity ($\epsilon = \Upsilon_{\Sigma\Gamma} / \Upsilon_\beta$); therefore, the void fraction is proportional to bubble Froude number ($Fr = U_{SG} / [g d_{32}]^{0.5}$). Assuming that void fraction scales as a power law function of Froude number (Equation 5), Archimedes number (Equation 9), and Eötvös number (Equation 10), then Equation (17) gives the general form of $G()$. The exponents in Equation (17) (i.e. X , Ψ , and Ω) were calculated from Equation (18) ($X= 1.117$, $\Psi= 0.1$, and $\Omega= -0.032$). Figure 12 shows that the proposed coordinates (see Equation 19) were able to successfully scale the void fraction within the heterogeneous regime. Equation (19) successfully predicts the void fraction within $\pm 25\%$ accuracy for the current data.

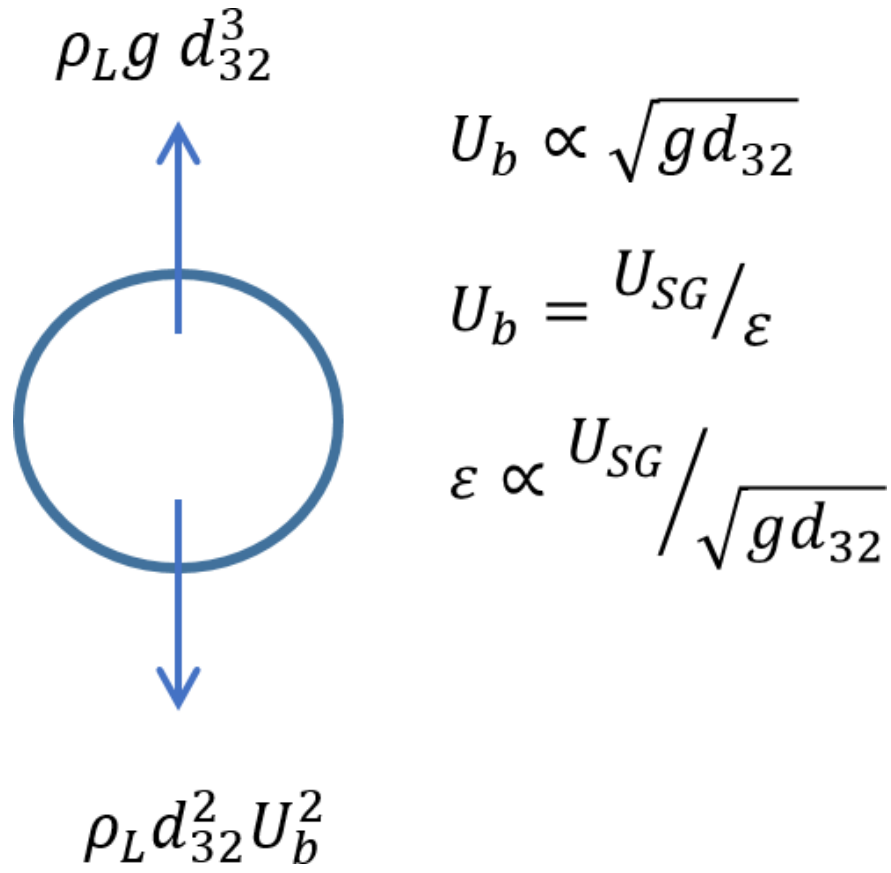


Figure 11 . Schematic of the primary acting forces on a single bubble at terminal velocity.

$$\varepsilon = A \text{Fr} \text{Ar}^\Psi \text{Eo}^\Omega \quad (17)$$

$$\frac{U_{SG}}{\sqrt{g d_{32}}} \cong \text{Fr} \text{Ar}^\Psi \text{Eo}^\Omega \quad (18)$$

$$\varepsilon = 0.035 (\text{Fr}^{1.117} \text{Ar}^{0.1} \text{Eo}^{-0.032})^{0.75} \quad (19)$$

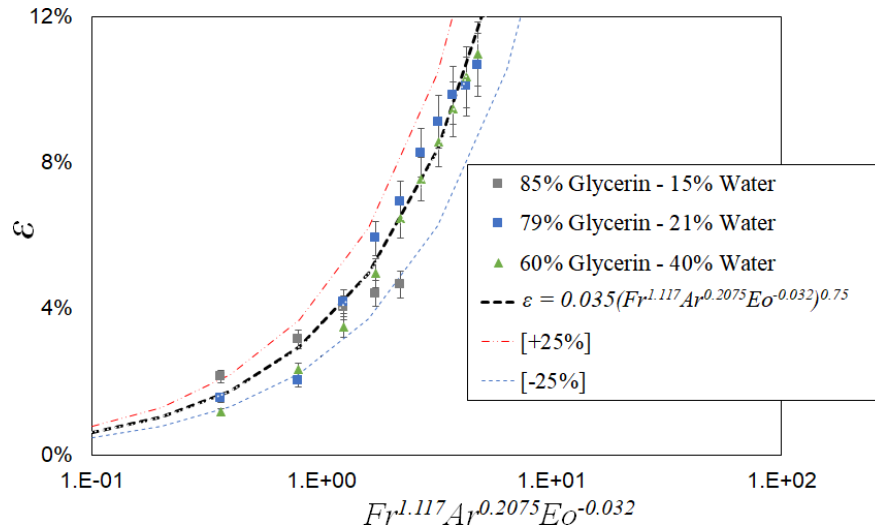


Figure 12 . A correlation for scaling the void fraction in the heterogeneous regime.

Conclusions

A systematic study of bubble size and void fraction in a batch bubble column with a porous sparger was carried out. The measurements (i.e. bubble size and void fraction) were carried out in homogenous and heterogeneous operation regimes. Bubble size measurements were performed using optical photography of large populations of bubbles (2400 and more). Void fraction was measured from the differential pressure across the bubble column height. Water and aqueous solutions of glycerin were used to test the effect of viscosity on the operation regime, bubble size, and void fraction. Gas superficial velocity was tested in the range of $6.9 \text{ mm/s} < U_{SG} < 69 \text{ mm/s}$ using compressed air. Regime transition corresponds to the change of physical behavior of the gas liquid system in bubble columns; therefore, it is appropriate to present any measurements with consideration of the operation regime. Current work uses PDF as well as probability plots to characterize the bubble size distribution in homogenous and heterogeneous operation regimes.

Results showed that in the homogenous regime, the bubble size distribution is poly-dispersed and the PDF exhibits Gaussian characteristics. In the heterogeneous regime, bubble coalescence events and shear breakage modified the bubble size distribution, results in the distribution approaching mono-dispersed as indicated by the PDF having a “spike” shape with a lognormal right leg.

Results also showed that increasing the viscosity accelerates the regime transition from homogenous to heterogeneous by allowing the formation of larger bubbles as well as bubble interaction (i.e. breakage and coalescence). Bubble size measurements were carried out in both operation regimes. In the homogenous regime, the characteristic bubble size (i.e. Sauter mean diameter) shows strong dependence on the sparger characteristics and injection condition due to the absence of breakage and coalescence. In the heterogeneous regime, experimental data exhibits a strong correlation between the Sauter mean diameter and specific input power (per unit mass). Dimensional analysis was used to propose a correlation between the scaled bubble size and the scaled specific input power. This correlation was validated against experimental data in literature both from static and vibrating bubble column studies. Void fraction was also measured in both the homogenous and heterogeneous regimes. As expected, the trend between void fraction and gas superficial velocity was dependent on the operation regime. Using dimensional analysis correlations for scaling the void fraction in homogenous and heterogeneous regimes were proposed and validated against experimental data.

Acknowledgments

The authors would like to thank Adam Still for the initial design and fabrication of the facility as well as assistance with the initial operation of it. This research was funded, in part, by B.R.E.'s Halliburton Faculty Fellowship endowed professorship.

Nomenclature

Symbol	Description	Unit
a	Bubble major axis	[mm]
A	Cross-sectional area	[mm ²]
AR	Bubble aspect ratio (ratio of the major to minor axis)	[-]
Ar	Archimedes number	[-]
BSD	Bubble size distribution	[-]
C	Proportionality coefficient	[-]
Ca	Capillary number	[-]
d	Bubble diameter	[mm]
D	Column diameter	[mm]
EO	Eötvös number	[-]
F	Force	[kgms ⁻²]
Fr	Froude number	[-]
g	Gravitational acceleration	[ms ⁻²]
k	Proportionality coefficient	[-]
Mo	Morton number	[-]
n	Number of bubbles in a sample population	[-]
Oh	Ohnesorge number	[-]
P	Input power from gas injection	[kgm ² s ⁻³]
PDF	Probability density function	[-]
Q	Volumetric flow rate	[m ³ s ⁻¹]
r	Average pore radius	[μm]
Re	Reynolds number	[-]
RMS	Standard deviation of bubble size distribution	[mm]
$S(d_b)$	Skewness of bubble size distribution	[mm]
U	Velocity	[mms ⁻¹]
We	Weber number	[-]
Greek letters and symbols	Greek letters and symbols	Greek letters and symbols
Symbol	Description	Unit
$[?]H$	Vertical distance between two pressure taps	[m]
$[?]p$	Differential pressure	[kg m ⁻¹ s ⁻²]
ϵ	Void fraction	[-]
$\kappa(\widehat{\delta}_\beta)$	Kurtosis of bubble size distribution	[-]
μ	Viscosity	[kgm ⁻¹ s ⁻¹]
ρ	Density	[kgm ⁻³]
σ	Surface tension	[kgs ⁻²]
X	Froude number exponent in Equation (17)	[-]
Ψ	Archimedes number exponent in Equation (17)	[-]
Ω	Eötvös number exponent in Equation (17)	[-]
Subscripts	Subscripts	Subscripts
10	Arithmetic mean diameter	

Symbol	Description	Unit
32	Sauter mean diameter	
95	Maximum stable bubble size	
b	Bubble	
B	Buoyancy force	
cap	Capillary	
cr	Critical	
D	Drag force	
eq	Equivalent	
G	Gas phase	
L	Liquid (phase)	
m	Specific value	
max	Maximum	
min	Minimum	
mf	Most frequent	
p	Porous sparger	
SG	Superficial gas	

References

- [1] Kantarci N, Borak F, Ulgen KO. Bubble column reactors. *Process Biochemistry*. 2005;40(7):2263-2283.
- [2] Shah YT, Kelkar BG, Godbole SP, Deckwer WD. Design parameters estimations for bubble column reactors. *AIChE Journal*. 1982;28(3):353-379.
- [3] Deckwer WD, Louisi Y, Zaidi A, Ralek M. Hydrodynamic properties of the Fischer-Tropsch slurry process. *Industrial & Engineering Chemistry Process Design and Development*. 1980;19(4):699-708.
- [4] Schumpe A, Grund G. The gas disengagement technique for studying gas holdup structure in bubble columns. *The Canadian Journal of Chemical Engineering*. 1986;64(6):891-896.
- [5] Saxena SC, Rao NS, Saxena AC. Heat-transfer and gas-holdup studies in a bubble column: air-water-glass bead system. *Chemical Engineering Communications*. 1990;96(1):31-55.
- [6] Daly JG, Patel SA, Bukur DB. Measurement of gas holdups and Sauter mean bubble diameters in bubble column reactors by dynamics gas disengagement method. *Chemical Engineering Science*. 1992;47(13-14), 3647-3654.
- [7] Pino LZ, Solari RB, Siquier S, Antonio Estevez L, Yopez MM, Saez, AE. Effect of operating conditions on gas holdup in slurry bubble columns with a foaming liquid. *Chemical Engineering Communications*. 1992;117(1):367-382.
- [8] Krishna R, De Swart JW, Ellenberger J, Martina GB, Maretto C. Gas holdup in slurry bubble columns: effect of column diameter and slurry concentrations. *AIChE Journal*. 1997;43(2):311-316.
- [9] Hyndman CL, Larachi F, Guy C. Understanding gas-phase hydrodynamics in bubble columns: a convective model based on kinetic theory. *Chemical Engineering Science*. 1997;52(1):63-77.
- [10] Luo X, Lee DJ, Lau R, Yang G, Fan, LS. Maximum stable bubble size and gas holdup in high-pressure slurry bubble columns. *AIChE journal*. 1999;45(4):665-680.
- [11] Li H, Prakash A. Analysis of bubble dynamics and local hydrodynamics based on instantaneous heat transfer measurements in a slurry bubble column. *Chemical Engineering Science*. 1999;54(21):5265-5271.

- [12] Lockett MJ, Kirkpatrick RD. Ideal bubbly flow and actual flow in bubble columns. *Transactions of the Institution of Chemical Engineers*. 1975;53:267–73.
- [13] Kara S, Kelkar BG, Shah YT, Carr NL. Hydrodynamics and axial mixing in a three-phase bubble column. *Industrial & Engineering Chemistry Process Design and Development*. 1982;21(4):584-594.
- [14] Koide K, Takazawa A, Komura M, Matsunga H. Gas holdup and volumetric liquid phase mass transfer coefficient in solid-suspended bubble column. *Journal of Chemical Engineering of Japan*. 1984;17:459–66.
- [15] Eissa SH, Schügerl K. Holdup and backmixing investigations in cocurrent and countercurrent bubble columns. *Chemical Engineering Science*. 1975;30(10):1251-1256.
- [16] Bach HF, Pilhofer T. Variation of gas holdup in bubble columns with physical properties of liquids and operating parameters of columns. *Ger Chemical Engineering*. 1978;1: 270–275.
- [17] Godbole SP, Honath MF, Shah YT. Holdup structure in highly viscous newtonian and non-newtonian liquids in bubble columns. *Chemical Engineering Communications*. 1982;16(1-6):119-134.
- [18] Khare AS, Joshi JB. Effect of fine particles on gas hold-up in three-phase sparged reactors. *Chemical Engineering Journal*. 1990;44(1):11-25.
- [19] Ruzicka MC, Drahoš J, Mena PC, Teixeira JA. Effect of viscosity on homogeneous–heterogeneous flow regime transition in bubble columns. *Chemical Engineering Journal*. 2003;96:15–22.
- [20] Olivieri G, Russo ME, Simeone M, Marzocchella A, Salatino P. Effects of viscosity and relaxation time on the hydrodynamics of gas–liquid systems. *Chemical Engineering Science*. 2011;66(14):3392-3399.
- [21] Rabha S, Schubert M, Hampel U. Regime transition in viscous and pseudo viscous systems: A comparative study. *AIChE Journal*. 2014;60(8):3079-3090.
- [22] Besagni G, Inzoli F, De Guido G, Pellegrini LA. The dual effect of viscosity on bubble column hydrodynamics. *Chemical Engineering Science*. 2017;158:509-538.
- [23] Besagni G, Inzoli F, Ziegenhein T. Two-phase bubble columns: A comprehensive review. *ChemEngineering*. 2018;2(2):13.
- [24] Akita K, Yoshida F. Gas holdup and volumetric mass transfer coefficient in bubble columns. Effects of liquid properties. *Industrial & Engineering Chemistry Process Design and Development*. 1973;12(1):76-80.
- [25] Mersmann A. Design and scale-up of bubble and spray columns. *Ger Chemical Engineering*. 1978;1:1–11.
- [26] Riquarts HP, Pilhofer T. Modell des heterogenen Strömungszustandes in Blasensäulen. *Verfahrenstechnik*. 1978;12:77-80.
- [27] Iordache OM, Muntean OI. Stochastic approach to the hydrodynamics of gas-liquid dispersions. *Industrial & Engineering Chemistry Fundamentals*. 1981;20(3):204-207.
- [28] Santus D, Salvagno N. Purificazione di gas naturale da composti acidi mediante assorbimento fisico downhole. 2014; Master’s Thesis, Politecnico di Milano, Milan, Italy.
- [29] Leonard C, Ferrasse JH, Boutin O, Lefevre S, Viand A. Bubble column reactors for high pressures and high temperatures operation. *Chemical Engineering Research and Design*. 2015;100:391-421.
- [30] Li H, Prakash A. Influence of slurry concentrations on bubble population and their rise velocities in a three-phase slurry bubble column. *Powder Technology*. 2000;113(1-2):158-167.
- [31] Deckwer WD. *Bubble Column Reactors*. Chichester, UK: John Wiley & Sons Ltd., 1992.
- [32] Manoharan S, Jog MA, Manglik RM. Effects of liquid viscosity on bubble growth from submerged orifice plates. American Society of Mechanical Engineers. In ASME 2017 Heat Transfer Summer Conference (pp. V002T11A012-V002T11A012).

- [33] Wilkinson PM, Spek AP, van Dierendonck LL. Design parameters estimation for scale-up of high-pressure bubble columns. *AIChE Journal*. 1992;38(4):544-554.
- [34] Kuncova G, Zahradnik J. Gas holdup and bubble frequency in a bubble column reactor containing viscous saccharose solutions. *Chemical Engineering and Processing Process Intensification*. 1995;34:25-34.
- [35] Lange V, Azzopardi BJ, Licence, P. Hydrodynamics of ionic liquids in bubble columns. In *Ionic Liquids- New Aspects for the Future*; InTechOpen: London, UK, 2013.
- [36] Philip J, Proctor JM, Niranjana K, Davidson JF. Gas hold-up and liquid circulation in internal loop reactors containing highly viscous newtonian and non-newtonian liquids. *Chemical Engineering Science*. 1990;45:651-664.
- [37] Yang JH, Yang JI, Kim HJ, Chun DH, Lee HT, Jung H. Two regime transitions to pseudo-homogeneous and heterogeneous bubble flow for various liquid viscosities. *Chemical Engineering and Processing Process Intensification*. 2010;49:1044-1050.
- [38] Hinze JO. Fundamentals of the hydrodynamic mechanism of splitting in dispersion processes. *AIChE Journal*. 1955;1(3):289-295.
- [39] Mouza AA, Dalakoglou GK, Paras SV. Effect of liquid properties on the performance of bubble column reactors with fine pore spargers. *Chemical Engineering Science*. 2005;60(5):1465-1475.
- [40] Kazakis NA, Papadopoulos ID, Mouza AA. Bubble columns with fine pore sparger operating in the pseudo-homogeneous regime: gas hold up prediction and a criterion for the transition to the heterogeneous regime. *Chemical Engineering Science*. 2007;62(12):3092-3103.
- [41] Besagni G, Di Pasquali A, Gallazzini L, Gottardi E, Colombo LPM, Inzoli F. The effect of aspect ratio in counter-current gas-liquid bubble columns: Experimental results and gas holdup correlations. *International Journal of Multiphase Flow*. 2017;94:53-78.
- [42] Houghton G, McLean AM, Ritchie PD. Mechanism of formation of gas bubble-beds. *Chemical Engineering Science*. 1957;7(1-2):40-50.
- [43] Abramoff MD, Magalhaes PJ, Ram SJ. Image processing with ImageJ. *Biophotonics International*. 2004;11(7):36-42.
- [44] Peters R, Rasband WS. ImageJ, US National Institutes of Health, Bethesda, Maryland, USA. 2012.
- [45] Schneider CA, Rasband WS, Eliceiri KW. NIH Image to ImageJ: 25 years of image analysis. *Nature Methods*. 2012;9(7):671.
- [46] Rasband WS. ImageJ. U.S. National Institutes of Health, Bethesda, MD, USA, 1997-2016. Available online: <http://imagej.nih.gov/ij> (accessed on 16 April 2013).
- [47] Mohagheghian S, Elbing BR. Characterization of Bubble Size Distributions within a Bubble Column. *Fluids*. 2018;3 (1):13.
- [48] Mohagheghian S, Still AL, Elbing BR, Ghajar AJ. Study of bubble size, void fraction, and mass transport in a bubble column under high amplitude vibration. *ChemEngineering*. 2018;2 (2):16.
- [49] Mohagheghian S, Ghajar AJ, Elbing BR. Effect of vertical vibration on the mixing time of a passive scalar in a sparged bubble column reactor. *Fluids*. 2020;5(1):6.
- [50] Anastasiou AD, Kazakis NA, Mouza AA, Paras SV. Effect of organic surfactant additives on gas holdup in the pseudo-homogeneous regime in bubble columns equipped with fine pore sparger. *Chemical Engineering Science*. 2010;65(22):5872-5880.
- [51] Alves SS, Maia CI, Vasconcelos JMT, Serralheiro AJ. Bubble size in aerated stirred tanks. *Chemical Engineering Journal*. 2002;89 (1-3):109-117.

[52] Lewis D, Davidson JF. Bubble splitting in shear flow. *Transactions of the Institution of Chemical Engineers*. 1982;60:283–291.

[53] Waghmare YG, Dorao CA, Jakobsen HA, Knopf FC, Rice RG. Bubble size distribution for a bubble column reactor undergoing forced oscillations. *Industrial & Engineering Chemistry Research*. 2009;48(4):1786-1796.